General Disclaimer

One or more of the Following Statements may affect this Document

- This document has been reproduced from the best copy furnished by the organizational source. It is being released in the interest of making available as much information as possible.

- This document may contain data, which exceeds the sheet parameters. It was furnished in this condition by the organizational source and is the best copy available.

- This document may contain tone-on-tone or color graphs, charts and/or pictures, which have been reproduced in black and white.

- This document is paginated as submitted by the original source.

- Portions of this document are not fully legible due to the historical nature of some of the material. However, it is the best reproduction available from the original submission.

Laboratory for Space Physics

Department of Physics
Washington University/St. Louis

LARGE-AREA PULSE IONIZATION CHAMBER FOR MEASUREMENT OF EXTREMELY HEAVY COSMIC RAYS*

J. W. EPSTEIN, J. L. FERNANDEZ, M. H. ISRAEL,† J. KLARMANN, and R. A. MEWALDT
Department of Physics, Washington University, St. Louis, Mo. 63130

W. R. BINNS
McDonnell Douglas Research Laboratories, St. Louis, Mo. 63166

*Work supported in part by the National Aeronautics and Spcae Administration under grant NGR-26-008-001 and in part by McDonnell Douglas Corporation, Independent Research and Development Program.

†Alfred P. Sloan Research Fellow

Abstract

Parallel-plate ionization chambers with nearly 1 m^2 active area have been constructed and successfully operated in a series of high-altitude balloon flights. The chambers are used for identification of relativistic cosmic-ray nuclei with charge greater than or equal to 20. For relativistic iron nuclei [charge 26] the charge resolution [FWHM] achieved is 5.5 percent [i.e., less than 1.5 charge units].

Introduction

We have constructed parallel-plate ionization chambers with nearly 1 m^2 active area, and have successfully operated them during five high-altitude balloon flights of a new cosmic-ray detector system. This system is designed to determine the charge spectrum of very-very-heavy [VVH] cosmic rays, i.e., cosmic-ray nuclei with charge, Z, greater than 30. The ionization chambers measure the energy loss of particles penetrating the system, a quantity proportional to the square of the charge, and so provide information for determining Z.

Since the discovery of VVH cosmic-ray tracks in meteorites[1], it has been apparent that the very low flux of these cosmic rays would require very large detectors for investigations of the contemporary radiation. To date, studies of contemporary VVH cosmic rays have been performed with balloon-borne passive detectors, i.e., either nuclear emulsions[2] or a combination of emulstions and plastic track detectors.[3] We have turned to active [i.e., electronic] detectors for VVH studies because such instruments are suitable for unmanned, unrecoverable satellites, thereby providing long collection times outside the atmosphere. Also, these new detectors should provide a completely independent measurement of the VVH cosmic-rays. For example, we hope to resolve the question of the existence of nuclei much heavier than uranium.[2,4]

Ionization chambers are well suited for energy-loss measurements of highly charged cosmic rays. They introduce a minimum of material into the particle beam, thereby reducing the loss of particles by nuclear interactions. Furthermore, they are appropriate for measuring the very large ionization of VVH cosmic rays. Typical applications of ionization chambers have involved stopping alpha particles of the order of 5 MeV and fission fragments of the order of 100 MeV. In a 5-cm argon-filled ionization chamber, 5 MeV is the energy deposited by a relativistic nucleus of charge 20; while 100 MeV is the energy deposited by a relativistic nucleus of

charge near 92. Thus we expect ionization chambers to operate effectively and linearly for VVH as well as VH [$20 \leq Z \leq 30$] cosmic rays. [Plastic scintillator, another energy-loss detector which is easily constructed in large areas, displays significant saturation for relativistic nuclei with charge below 26[5, 6], and so is not likely to be suitable for nuclei of higher charge.]

Small [300 cm^2] pulse ionization counters have been used in a balloon-borne detector system to measure the composition of the more abundant cosmic rays with $Z<30$.[7] Our chambers are constructed differently and are significantly larger [9800 cm^2].

In this paper, we shall discribe briefly the complete system in which these ionization chambers are used, describe in detail the construction of the chambers and the laboratory tests of their operation, present balloon-flight results indicating the charge resolution, and compare the observed response of the chambers with calculations.

Preliminary results from our first successful flight of the system were presented at the Washington, D. C., meeting of the Division of Cosmic Physics of the American Physical Society,[8] and further scientific results will be published shortly.

Complete Detector System

Figure 1 is a schematic cross-section of our detector system. The principal components of the system are the two ionization chambers and the Cerenkov counter. The pulse height from each of these three detectors is recorded for each heavily charged particle that penetrates the system. The trajectory of the particle is given by the hodoscope consisting of two crossed layers of scintillator strips above and two crossed layers below the other counters.

The radiator of the Cerenkov counter is a sheet of ultra-violet-transmitting [UVT] Lucite, 1 m x 1 m x 6.35mm. Light collection is by total internal reflection, with the radiator viewed on each of its four edges by a 12.7-cm

diameter, photomultiplier tube [RCA 4525] with an adiabatic light-pipe of UVT Lucite. The outputs of the four tubes are added to give a single Cerenkov signal. A similar counter of somewhat smaller area [0.5 m x 0.5 m] has recently been described,[9] and we shall not describe our counter further. [A modified counter using diffuse light collection in a white box instead of total internal reflection was used in our most recent flight but results from that flight are not yet available.]

Each layer of the hodoscope consists of ten strips of plastic scintillator [Pilot Y], each 1.09 m x 95 mm x 1.6 mm. The overlap of two such layers, one rotated 90° from the other, defines a 0.95 m x 0.95 m active area, divided into 100 equal squares. Each scintillator strip is viewed by a single photomultiplier tube [RCA 6199] near one end. In a typical strip, the light collection varies by a factor of 2.5 between the near and far ends of the 0.95 m active length. A discriminator is triggered whenever the photomultiplier signal exceeds by a factor of 50 the signal due to a single relativistic muon passing vertically through the far end of the strip.

A six-fold coincidence triggers the recording of an event. The coincidence circuit requires a discriminator output from at least one strip in each of the four hodoscope layers, and also an output from each of the ionization-chamber discriminators. [The latter are typically set for a threshold corresponding to a vertical passage of a relativistic nucleus of charge near 16 through the chamber.] For each event, the pulse heights from each of the ionization chambers and from the Cerenkov counter are recorded. Also, the trajectory of the particle is indicated by recording which hodoscope-strip discriminators were triggered.

There are four guard counters, one on each side of the detector square. Each guard counter is a 1.02m x 0.25m x 9.5 mm sheet of plastic scintillator [NE 110], viewed directly by a photomultiplier [RCA 6199]. A discriminator on each output has threshold at approximately 30 times the output for a relativistic muon passing horizontally through the counter far from

the phototube. The guard counters are not used in active anti-coincidence; rather, for each event the system records the triggering of each guard discriminator.

The entire detector system and electronics are enclosed in an aluminum sphere, 1.8 m in diameter, 2 mm thick, which maintains the equipment at 1-atmosphere pressure throughout the balloon flight.

Ionization Chamber Construction

Figure 2 is an exploded view of one ionization chamber. It is a self-contained, gas-tight box with inside dimensions 0.99 m x 0.99 m x 51 mm. The aluminum high-voltage electrodes form the top and bottom of the box; the strips of glass-epoxy insulator, which separate the electrodes, form the four walls of the box.

We require electrodes whose thickness is small compared to the interaction length of the heaviest nuclei [$\sim$4 cm in aluminum] and whose structural strength is sufficient to support themselves over 1 m^2 and to contain the gas reliably inside the chamber. Each electrode is constructed as a sandwich of two sheets of 0.13 mm aluminum glued on opposite sides of a 13 mm sheet of plastic foam [Dow Dorvon density 0.016 g/cm^3]. The resulting sandwich is rigid but has low areal density, 0.09 g/cm^2.

The walls of the chamber are 13 mm thick strips of glass-epoxy board [Formica FF 91] screwed together. The joints between the sides are sealed with epoxy [Scotch Weld No. 2216a-B] which makes a strong but slightly flexible joint and the electrodes are connected and sealed to the sides with fillets of the same epoxy. The fully assembled chamber weighs 9 kg.

A 20 nanocurie americium-241 source of 5.5 MeV alpha particles is attached to the negative electrode of each chamber as shown in Figure 3. Mounting the source a short distance away from the hole in the electrode results in a beam of alpha particles which is collimated to within 45^o of the normal to the electrode. Collimation of the beam produces a peaked pulse-height distribution, as described in a later paragraph. In the gas mixture

we use, 5.5 MeV alpha particles have a range of 4.31 cm.

In mounting the chambers it is necessary, in order to reduce the electronic noise, to minimize the capacitance between the collecting electrodes of the two chambers and between either collecting electrode and ground. Thus the chambers are separated as indicated in Fig. 1. An aluminum rf shield completely encloses both chambers and the associated preamplifiers. The chambers are mounted with the ground electrodes to the outside, with the outer 0.13 mm aluminum sheet of the ground electrode sandwiches forming the top and bottom of the rf shield. The remainder of the shield is of .51 mm aluminum sheet.

Gas

The chambers are operated at atmospheric pressure with a mixture of 90 percent argon and 10 percent methane, a mixture commonly used in ionization chambers. During balloon flights, we continuously flush fresh gas through the chamber at a rate of approximately 100 liters [the total volume of the two chambers] per 20 hours.

Chamber operation is not harmed by some contaminants in the gas, but trace amounts of other contaminants can have extremely adverse effects. Our gas is mixed commercially from contamination-free argon and C. P. - grade methane. Analysis by the supplier has shown that the gas mixture we have used successfully has a typical contamination of approximately 200 ppm of nitrogen, 200 ppm of ethane, 2 ppm of oxygen, and less than 1 ppm of water vapor.

However, gas from two defective cylinders was incapable of giving any measurable signal in our chambers. The supplier's subsequent analysis of the gas in one of those cylinders showed a contamination of 4 ppm of sulfur hexafluoride, although their typical gas has less than 0.1 ppm of this contaminant. We estimated the concentration of SF_6 which significantly affects the chambers by noting the drop in signal as gas from this contaminated bottle was slowly introduced into an operating chamber. The

signal dropped to half its normal value when the SF_6 concentration was somewhere between 0.5 and 1.0 ppm. With 2 ppm of SF_6 there was no detectable signal.

The chambers are ordinarily operated with a continuous gas flow, but we have made limited tests with the chambers sealed. After several months of chamber operation with almost continuous flow, we found that the chamber could operate without gas flow for a week with less than 2 percent decrease in the amplitude of the source calibration signal; however, neither the selection of construction materials nor their treatment prior to assembly of the chamber were designed for optimum cleanliness. Glass-epoxy board outgasses more than some other dielectrics. In cleaning the materials, we used standard solvents, trichloroethylene and methyl alcohol, but no bake-out or ultrasonic cleaning was performed.

Signal Characteristics

The chamber is operated in the electron pulse mode. The differentiating time-constant of the preamplifier-amplifier combination on the chamber is 5 μsec. This time-constant is longer than the electron collection time [less than 1 μsec] and very short compared to the positive-ion collection time [several m sec]. A positive d.c. high voltage, normally 600 volts, is applied to the chamber. The anode is connected to the [capacitively coupled] input of a charge-sensitive preamplifier [Hewlett-Packard 5554A].

All laboratory testing of the chambers and associated electronics is done with the internal Am^{241} α-source in each chamber. Calculations indicate that the signal corresponding to the mean of the α-distribution is the same as that due to the transversal of a vertically incident, relativistic nucleus of charge 21.5. This fact allows the adjustment of the gains and discriminator levels of the ion chamber electronics in the absence of a beam of relativistic high Z particles for ground testing.

The 600 V operating point is on a wide plateau where the chamber's output is quite insensitive to large changes in the applied voltage. The pulse rise-

time [10 percent to 90 percent of peak voltage] at the preamplifier output varies by less than 15 percent for operating voltages from 400 to 1000 V. At 600 V the rise-time is 0.7 μsec. The rise-time increases to 1.5 μsec at 200 V and 4 μsec at 100 V. The observed variation of rise-time with voltage is in very good agreement with the variation expected from experimental[10] values of electron drift velocity in a mixture of 90 percent argon with 10 percent methane. Similarly, the measured pulse-heights from our alpha-particle calibration source vary by less than 3 percent as the operating voltage varies between 300V and 1000 V.

Response to Relativistic Nuclei

The pulse height resolution of an ionization chamber detecting fast charged particles is governed principally by the intrinsic fluctuations in the energy-loss process in a thin detector. Additional smaller contributions to the resolution of the chambers are intrinsic amplifier noise and path-length uncertainties introduced by the finite spatial definition of our hodoscope.

The ionization process in argon requires an average energy of approximately 30 eV to create a single electron-ion pair. With 5 MeV deposited in the chamber, approximately 2×10^5 electron-ion pairs are produced. Thus, statistical fluctuations in the number of pairs formed for a given energy loss are of the order of 0.2 percent, which is negligible compared to the other sources of fluctuation.

In calculating the pulse-height resolution for relativistic particles, it is essential to distinguish between the energy-loss of a charged particle as it penetrates the gas of the chamber and the energy-deposit in the chamber gas. [It is the energy-deposit which is directly related to the signal on the chamber output.] Energy-loss fluctuations include a contribution from the small but finite probability that a single electron in the gas be given an energy comparable to the average energy-loss. As a result, the statistical distribution of energy-loss is asymmetric, having a long tail [the "Landau tail"] toward the high energy loss.[11] On the other hand, in considering the

energy-deposit in a thin detector, the occasional energetic knock-on electron formed in the detector typically loses only a small fraction of its energy in the detector. The thickness of gas in one of our chambers is 8.5 mg/cm^2. So a 1 MeV electron, for example, if created near the center of the chamber, will contribute the order of 10 keV to the energy-deposit in the chamber, although it contributes 1 MeV to the energy-loss in the chamber. [This distinction between energy loss and energy deposit has been pointed out previously for thin scintillation and Cerenkov counters by Lund and Risbo.[12]]

Since the contribution to the energy-deposit by any one knock-on electron is small compared to the average energy-deposit in the chamber, the statistical distribution of energy-deposit will be nearly Gaussian, instead of assymmetric. Of course, the energy-deposit will have a contribution from energetic knock-on electrons created in the material above the chamber gas which then pass through the chamber. Like the energetic electrons created in the chamber, these electrons, leaking in from above, can each contribute only a small fraction of the average energy-deposit, so the energy-deposit distribution remains approximately Gaussian.

In our detector system there is approximately 1.1 g/cm^2 of material above the first ionization chamber. As shown in the Appendix, a good approximation for the mean square deviation due to energy-deposit fluctuations (σ_Δ^2) in this case is:

$$\sigma_\Delta^2 = \xi\eta \ln \frac{E_m}{\eta}$$

where $$\xi = \frac{0.3\ mc^2}{\beta^2} \frac{Z}{A} z^2 x$$

$$= 0.435 \text{ MeV for a 2.5 GeV/n iron nucleus incident normally in our chambers}$$

[2.5 GeV/n (7.0 GV) is approximately the median energy of iron nuclei incident on our detector during a balloon flight where the geomagnetic cutoff is 4.5 GV.]

η = energy of electron whose practical range is the thickness of the gas in the chamber

= 0.08 MeV in our chamber

E_m = maximum possible energy transfer to a single knock-on electron

= 12.8 MeV for a 2.5 GeV/n nucleus.

Thus for a typical iron nucleus incident on one chamber, we expect

$$\sigma_\Delta = 0.42 \text{ MeV}.$$

The mean energy-loss of a normally incident 2.5 GeV/n iron nucleus in one of our chambers is 8.90 MeV [using tabulated energy-loss for protons from Barkas and Berger [1964] multiplied by $[26]^2$]. We have calculated that the difference between the mean energy-deposit in the chamber and the mean energy-loss is approximately 1 percent, i.e., that portion of energy-loss [approximately 15 percent] which is carried out of the chamber by energetic knock-on electrons is very nearly equaled by energy deposited by knock-on electrons from the material above the chamber. Thus, we take 8.9 MeV as the mean energy-deposit, E_Δ from a 2.5 GeV/n iron nucleus; and we have σ_Δ equal to 4.7 percent of E_Δ.

Before comparing this calculated width with our observations, we must consider the other sources of pulse-height fluctuations, amplifier noise and path length uncertainty. Using a precision pulser on the test input of the charge sensitive preamplifiers, we found that the width of the output pulse-height distribution due to amplifier noise was characterized by σ_n equal to 2.2 percent of the mean pulse height due to normally incident relativistic iron. For any observed particle, the measured pulse-height from the ionization chambers was corrected by a factor sec Θ, where Θ is our best estimate of the angle between the particle's trajectory and the normal to the plates of the chamber. The finite resolution of the hodoscope gives an uncertainty in Θ which produces an error in the corrected pulse-height, characterized by σ_L equal to 2.1 percent.

Combining these three sources of pulse-height fluctuation gives, for a beam of relativistic iron nuclei, a predicted pulse-height distribution with σ equal to 5.6 percent, or full-width-at-half maximum [FWHM] 13.2 percent. Figure 4 displays the observed pulse height spectrum for each of the two ionization chambers derived from a half hour of flight data gathered at 4.5 g/cm^2 atmospheric depth near Palestine, Texas, where the vertical geomagnetic cutoff was 4.4 GV. Our in-flight pulse-height-analyzer has a response proportional to the square-root of the input pulse-height; therefore, the channel numbers on the x-axis are proportional to the square-root of the pulse-height and are directly proportional to the charge of a relativistic nucleus. The FWHM of the peak centered on channel 116 is approximately 7 to 8 percent in each case, corresponding to a 14 to 16 percent FWHM in pulse-height. This result is in reasonably good agreement with the predicted 13 percent. The added width of the observed peaks can be explained by a small number [approximately 10 percent] of nuclei of charge 25 and 27 included in the "iron" peak.

Two additional possible contributions to the width of the iron peak have been considered. [1] Variations in the response of the chamber as a function of position make a negligible contribution to the charge resolution. The variation in the mean of the iron peak was investigated over the 1 m^2

area of each chamber by sorting 850 iron events into a 5 x 5 grid using the hodoscope information. The maximum pulse height variation of the mean for any section of the grid was less than 3 percent from the mean of all iron events. Both chambers showed a systematic radial variation ranging from +1 percent at the center to -1 percent around the edge. These non-uniformities can be corrected for using the hodoscope information, but this has not yet been done since the contribution to the width of the peak corresponds to a σ_u of less than 1 percent. [2] The spread in velocities of the incident particles also has a negligible effect on the charge resolution. For relativistic nuclei above about 1.5 GeV/nucleon, the energy loss is nearly constant as a function of energy. The geomagnetic cutoff excludes particles with energy loss more than 5 percent larger than minimum ionizing particles. The relativistic rise of energy-loss introduces a tail on the high side of the distribution; but, because of the steep slope of the cosmic ray energy spectrum, does not significantly affect the width.

Figure 5 is a histogram of the mean of the two ionization chamber pulse heights for the same set of events. The iron peak in this case has FWHM of about $5\frac{1}{2}$ percent. This peak is narrower than the peaks of the individual chambers by a factor of approximately $\sqrt{2}$, as would be expected if the width is due principally to uncorrelated fluctuations in the two chambers.

Note also, that while the iron peak in Figure 5 is narrower than in either histogram of Figure 4, the number of events near charge 28 is nearly the same. This agreement implies that the events of pulse height corresponding to charge 28 are indeed due to particles of energy-loss higher than that of 2.5 GeV/n iron, not just due to statistical fluctuations in the pulse-height from iron nuclei. This correlation of high pulse heights in the two chambers is also demonstrated in Figure 6, a scatter plot of pulse-height in ion chamber 1 vs pulse height in ion chamber 2. [Note that in order to determine which of these higher events is due to nuclei of charge 28 and which due to extremely relativistic nuclei of charge 26 on the "relativistic rise" of ionization, analysis comparing the ionization and Cerenkov counter outputs is required. This analysis is in process.]

In-flight Calibration

During the balloon flight, the electronic system spends one minute every 34 minutes calibrating each ionization chamber. In the calibration mode, the requirement for recording an event is changed from a six-fold coincidence to a "one-fold coincidence" in which an event is recorded whenever one ionization chamber gives a signal above its discriminator threshold. During each one-minute calibration an alpha-particle spectrum containing approximately 130 events is recorded.

Figure 7 is the combined histogram of ionization chamber pulse-heights from two calibration periods of each chamber, recorded in flight immediately before and after the cosmic-ray events which were displayed in Figures 4, 5, 6. The solid curve drawn through the histogram is the calculated pulse-height distribution, incorporating the geometry of the alpha-particle source and the Gaussian noise of the preamplifier. The area under the calculated curve has been normalized to the total number of events in the histogram. Also, the position of the mean of the curve was normalized to the observed position. The width and shape of the curve were given by the calculation with no free parameters. [The counts outside the peak are due to electronic noise and do not significantly affect our measurements.]

The width of this curve is not a measure of the intrinsic resolution of the ionization chamber. Rather the width is primarily caused by wide collimation of the alpha-particle source. While the source is monoenergetic, the 45^{o} collimation permits the distribution of the 5.5 MeV energy-deposit to vary from particle to particle. The particles traveling perpendicular to the plates deposit their energy closer to the collecting electrode than do particles traveling at some angle. With the chamber acting in the electron-pulse mode, the signal is larger when the ionization occurs farther from the collecting electrode.

The alpha-particle calibration peak permits an absolute calibration of the observed cosmic-ray charge spectrum. Calculations show that the signal at the mean of the alpha calibration curve should have the same pulse height as a vertically incident cosmic-ray nucleus of 2.5 GeV/n of charge

21.5 ± 0.4. The uncertainty in this number is principally due to uncertainty in the distribution of energy loss along the path of a stopping alpha-particle, and also due to uncertainties in the precise energy-loss vs. energy relationships for relativistic heavy nuclei. The quoted uncertainty is a conservative estimate; we are confident that the correct value is within these limits. Using the in-flight calibration curve, this calculation implies that the mean of the peak in the cosmic-ray charge spectrum near channel 116 is at charge 26.1 ± 0.5. The width of the peak [approximately 1.3 charge units, FWHM] implies that it consists mostly of particles of one nuclear charge. We therefore have direct evidence that this peak consists of nuclei of $_{26}Fe$.

It is a pleasure to acknowledge the efforts of Mr. Kenneth Krippner and Mr. Arville J. Taylor whose work on the design and construction of the electronics was essential to the success of the experiment. We are also indebted to the crew of the NCAR Balloon Flight Station in Palestine, Texas, for splendid support of the balloon flights whose data is reported in this paper.

Appendix Energy-deposit Fluctuations

Consider an ionization counter of thickness x. Above the counter is a plate of thickness X. [All thicknesses and ranges are measured in g/cm^2.] Let E[R] = the energy of an electron whose practical range is R. [Practical range from Katz and Penfold.[13]]

Define

$$\eta = E(x)$$

$$H = E(X)$$

$$\xi = \frac{0.3\ m_e c^2}{\beta^2}\ \frac{Z}{A}\ z^2\ x$$

$$E_m = 2m_e c^2 \beta^2 \gamma^2$$

= maximum transferable energy from the incident particle to a single electron

where Z and A are the atomic number and atomic weight respectively of the detector gas

ze is the charge of the cosmic-ray particle

$m_e c^2$ is the rest energy of the electron (0.511 MeV)

β is the velocity of the particle in units of the velocity of light

$$\gamma^2 = (1 - \beta^2)^{-1}$$

We make the following simplifying assumptions:

1. Knock-on electrons with energy less than η created in the detector gas, lose all their energy in the gas.
2. Knock-on electrons with energy greater than η created in the detector gas, deposit energy η in the gas.
3. Knock-on electrons created in the plate above the chamber deposit η in the gas provided they reach the chamber with energy greater than η.
4. In determing whether an electron created in the plate does enter the chamber with energy greater than η, assume that electrons follow a range-energy relationship $R=aE$ [with a constant] [for $R \geq x$].
5. Ignore knock-on electrons entering the chamber from above with energy less than η.

Under these assumptions, fluctuations arise from three independent sources:

A] Knock-on electrons with energy less than η created in the detector gas.

B] Knock-on electrons with energy greater than η created in the detector gas.

C] Knock-on electrons entering the gas from above.

We now consider each of these sources in turn.

A] From Rossi[11] using equations 2.7.4, 2.7.8, and 2.3.6 we have for the mean square deviation in energy deposit due to low-energy electrons:

$$\sigma_A^2 = x \int_0^{\eta} E^2 \, \Phi_{col}(E)\, dE$$

where $\sigma_{col}(E)\,dE = \frac{\xi}{x}\frac{dE}{E^2}(1 - \beta^2 \frac{E}{E_m})$

= the probability per unit thickness of creating a knock-on electron with energy between E and E+dE

so

$$\sigma_A^2 = \xi\eta[1 - \frac{1}{2}\beta^2 \frac{\eta}{E_m}]$$

B] The number $[N_B]$ of knock-on electrons created in the chamber gas with energy greater than η is

$$N_B = x\int_{\eta}^{E_m} \Phi_{col}(E)\,dE = \xi[\frac{1}{\eta} - \frac{1}{E_m} - \frac{\beta^2}{E_m} \ell n \frac{E_m}{\eta}]$$

Since we assume that each of these electrons contribues an energy η to the chamber, the fluctuations here are due to Poisson fluctuations in the number N_B, so the mean square deviation in energy deposit due to these electrons is

$$\sigma_B^2 = \eta^2 N_B = \xi\eta[1 - \frac{\eta}{E_m}(1 + \beta^2 \ell n \frac{E_m}{\eta})]$$

C] Knock-on electrons created above the chamber and contributing to the energy deposit fluctuations in the chamber include N_1 electrons created in the plate with energy greater than $H + \eta$; and N_2 electrons created with energy, E, between η and H, created at locations less than $R[E-\eta]$ from the chamber. $R[E-\eta]$ is the

range of an electron of energy $E-\eta$. If we assume that Z/A for the plate above the chamber is the same as Z/A for the chamber gas, and we use assumption 4, we can show that

$$N_1 = \frac{\xi}{\eta} H \int_{H+\eta}^{E_m} dE \, \frac{1}{E^2}\left(1 - \beta^2 \frac{E}{E_m}\right)$$

$$= \frac{\xi}{\eta} \left[\frac{H}{H+\eta} - \frac{H}{E_m}\left(1 + \beta^2 \ln \frac{E_m}{H+\eta}\right)\right]$$

and

$$N_2 = \frac{\xi}{\eta} \int_{\eta}^{H+\eta} dE \left(\frac{E-\eta}{E^2}\right)\left(1 - \beta^2 \frac{E}{E_m}\right)$$

$$= \frac{\xi}{\eta} \left[\left(1 + \beta^2 \frac{\eta}{E_m}\right)\left(\ln \frac{H+\eta}{\eta}\right) - 1 + \frac{\eta}{H+\eta} - \beta^2 \frac{H}{E_m}\right]$$

As with σ_B, we assume that each of these electrons contributes an energy η, so the fluctuations in this case are Poisson fluctuations in the number $N_1 + N_2$, giving

$$\sigma_C^2 = \eta^2 (N_1 + N_2)$$

The distributions characterized by σ_A, σ_B, and σ_C will all be nearly Gaussian provided $\frac{\xi}{\eta} \gtrsim 10$, which is satisfied for our chambers. As a result, the energy deposit fluctuations will be nearly Gaussian and characterized by a mean square deviation given by

$$\sigma^2 = \sigma_A^2 + \sigma_B^2 + \sigma_C^2$$

$$= \xi\eta \left[2 + \ln \frac{H+\eta}{\eta} - \frac{H+\eta}{E_m}\left(1 + \beta^2 + \beta^2 \ln \frac{E_m}{H+\eta}\right) + \frac{\beta^2}{2} \frac{\eta}{E_m}\right]$$

For $\eta << E_m$ and $1-\beta^2 << 1$, this expression can be greatly simplified in two extreme cases. For negligible material above the chamber, i.e., $H << \eta$, we have simply

$$\sigma^2 = 2\,\xi\eta .$$

For a very thick plate above the chamber set $H = E_m$ and the expression reduces to

$$\sigma^2 = \xi\eta\ \ell n\ \frac{E_m}{\eta}$$

For our ionization chambers, with 1 g/cm^2 of material above them, the general expression gives a deviation only slightly less than the limiting case of a very thick plate, so the latter, simpler expression is used in the body of this paper.

Figure Captions

1. Schematic cross-section of the detector system.

2. Exploded view of one ionization chamber [not to scale].

3. Mounting of americium -241 calibration source on ground electrode of ion chamber. The alpha particles are collimated to 45^{o}.

4. Pulse-height histogram for each ionization chamber due to cosmic-ray nuclei. Data shown were gathered during a half hour of a balloon flight at 4.5 g/cm^2 atmospheric depth at 4.4 GV vertical geomagnetic cutoff. Pulse height scale is proportional to square-root of chamber's output pulse. Each pulse height was corrected by a factor Sec Θ, where Θ is the angle between the normal to the plates and the particle's trajectory.

5. Histogram of mean ionization chamber pulse height for same events shown in Figure 4.

6. Pulse height in chamber No. 1 vs pulse height in chamber No. 2 for some events shown in Figures 4 and 5. Legend o 1 event, • 2 or more events.

7. Pulse-height histogram due to 5.5 MeV alpha-particles from in-flight calibration. Solid curve is calculated pulse-height distribution normalized to total area and mean pulse-height of histogram.

References

1] R. L. Flesicher, P. B. Price, R. M. Walker, M. Maurette, and G. Morgan, J. Geophys. Res. 72 [1967] 355.

2] P. H. Fowler, V. M. Clapham, V. G. Cowen, J. M. Kidd, and R. T. Moses, Proc. Roy. Soc. Lond. A 318 [1970] 1.

3] G. E. Blanford, M. W. Friedlander, J. Klarmann, R. M. Walker, J. P. Wefel, W. C. Wells, R. L. Flesicher, G. E. Nichols, and P. B. Price, Phys. Rev. Letters 23 [1969] 338.

4] G. E. Blanford, R. L. Fleischer, P. H. Fowler, M. W. Friedlander, J. Klarmann, J. M. Kidd, G. E. Nichols, P. B. Price, R. M. Walker, J. P. Wefel, W. C. Wells, Acta Physica Hungaricae 29, suppl 1, [1970] 423.

5] G. D. Badhwar, C. L. Dency, B. R. Dennis, and M. F. Kaplon, Nucl. Instr. and Meth. 57 [1967] 116.

6] W. R. Webber, J. F. Ormes, and T. VonRosenvinge, Proc. 9th Intern. Conf. Cosmic Rays [1965] 407.

7] J. Engelman, L. Koch, J. P. Meyer, L. Sauvage, and D. DeZertucha, COSPAR, [Tokyo, 1968].

8] W. R. Binns, J. I. Fernandez, M. H. Israel, J. Klarmann, and R. A. Mewaldt, Bull. Am. Astron. Soc. 2 [1970] 287.

9] J. F. Ormes, V. K. Balasubrahmanyan, R. D. Price, M. J. Ryan, and R. F. Silverberg, IEEE Trans. Nucl. Sci. 17 [1970] 17.

10] W. N. English and G. C. Hanna, Can. J. Phys. 31 [1953] 768.

11] B. Rossi, High energy particles [Prentice Hall, Englewood Cliffs, N. J. 1952].

12] N. Lund and T. Risbo, Tech. Rept. CC1, Nov. 1965, Technical Univ. of Denmark.

13] L. Katz and A. S. Penfold, Rev. Mod. Phys. 24 [1952] 28.

FIG – 1

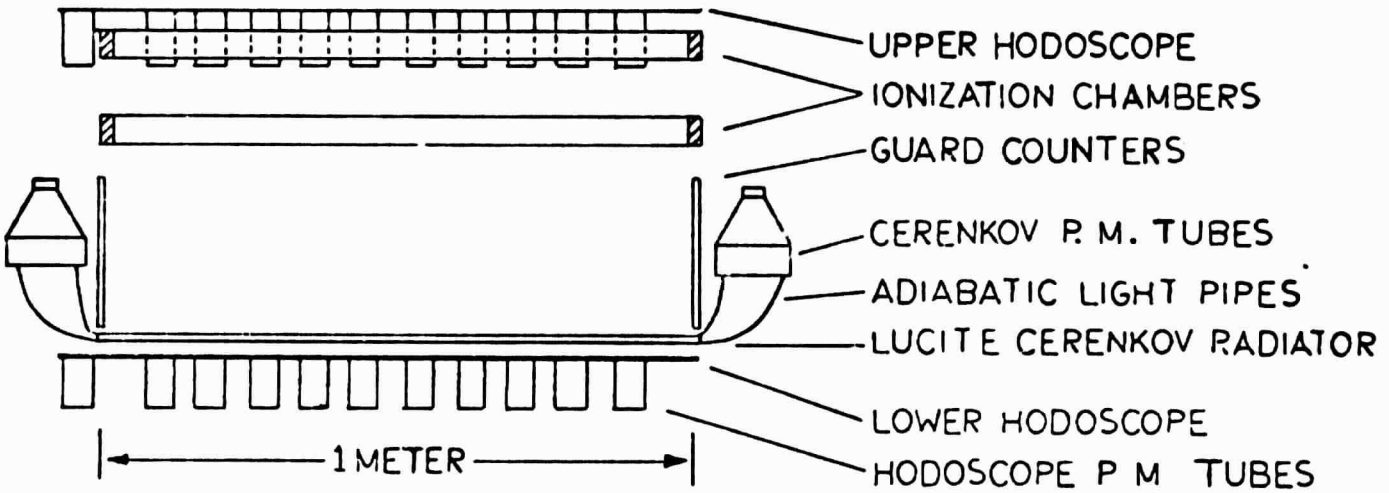
UPPER HODOSCOPE
IONIZATION CHAMBERS
GUARD COUNTERS
CERENKOV P. M. TUBES
ADIABATIC LIGHT PIPES
LUCITE CERENKOV RADIATOR
LOWER HODOSCOPE
HODOSCOPE P M TUBES
1 METER

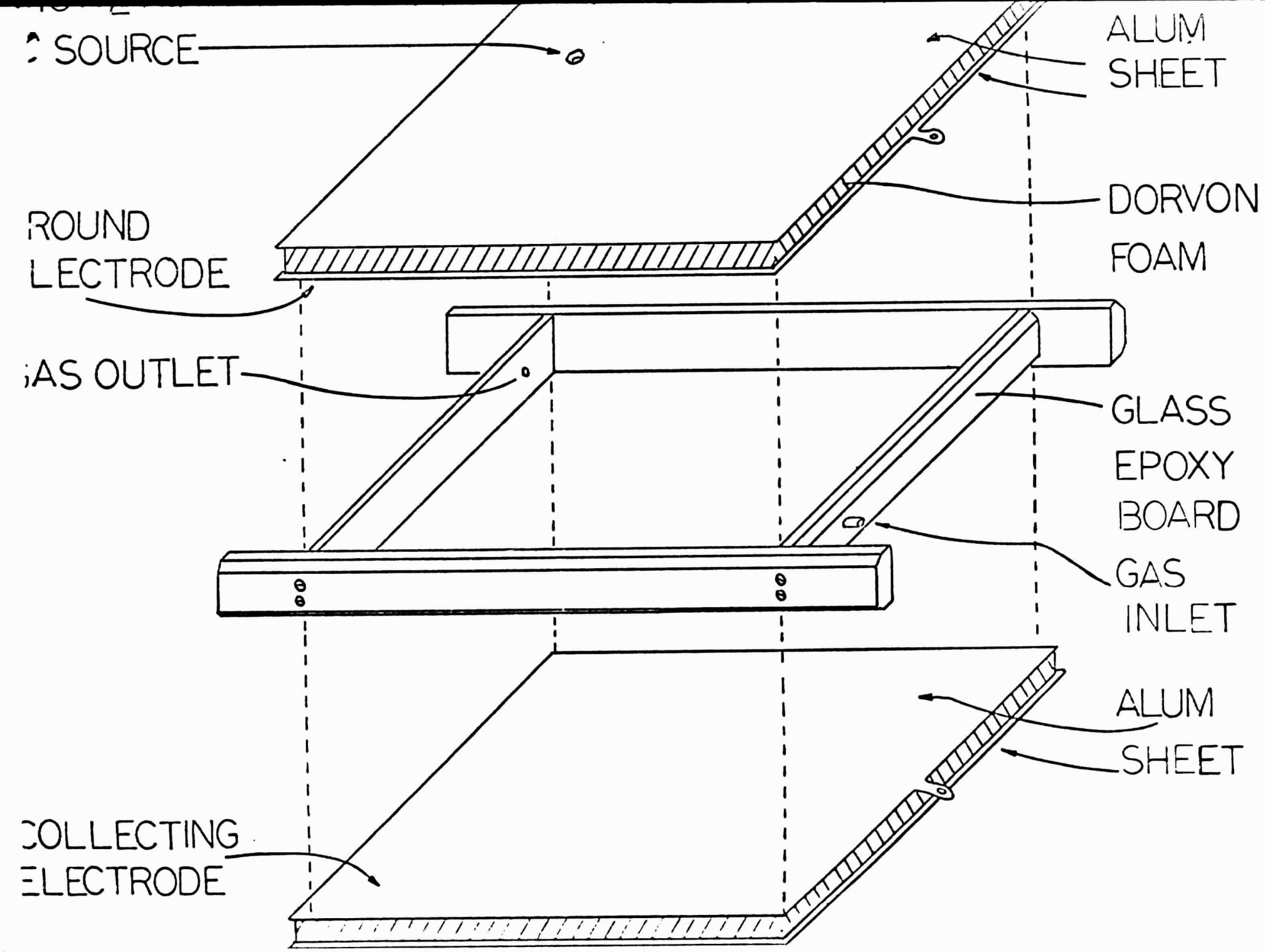
SOURCE
ALUM
SHEET
DORVON
FOAM
ROUND
LECTRODE
;AS OUTLET
GLASS
EPOXY
BOARD
GAS
INLET
ALUM
SHEET
COLLECTING
ELECTRODE

FIG -3

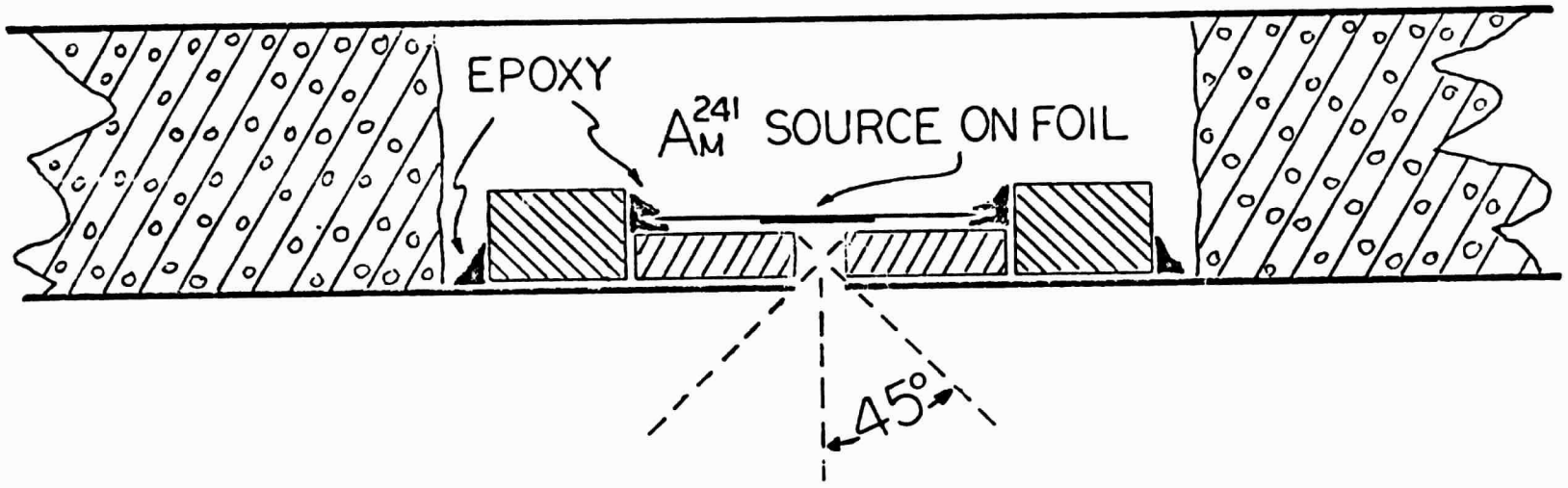

FIG - 4

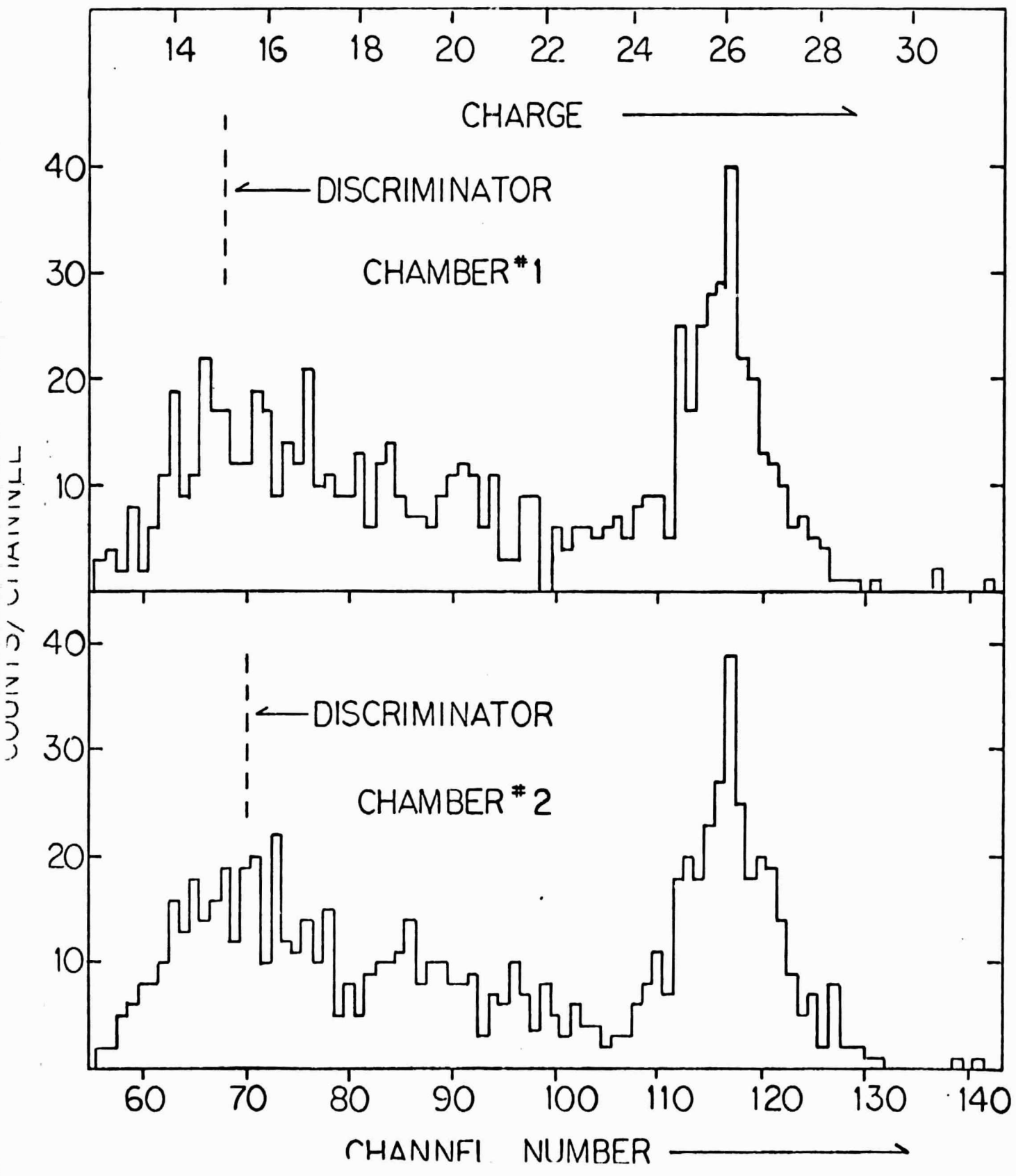
14
16
18
20
22
24
26
28
30
CHARGE
40
30
20
10
DISCRIMINATOR
CHAMBER #1
COUNTS/CHANNEL
40
30
20
10
DISCRIMINATOR
CHAMBER #2
60
70
80
90
100
110
120
130
140
CHANNEL NUMBER

FIG -5

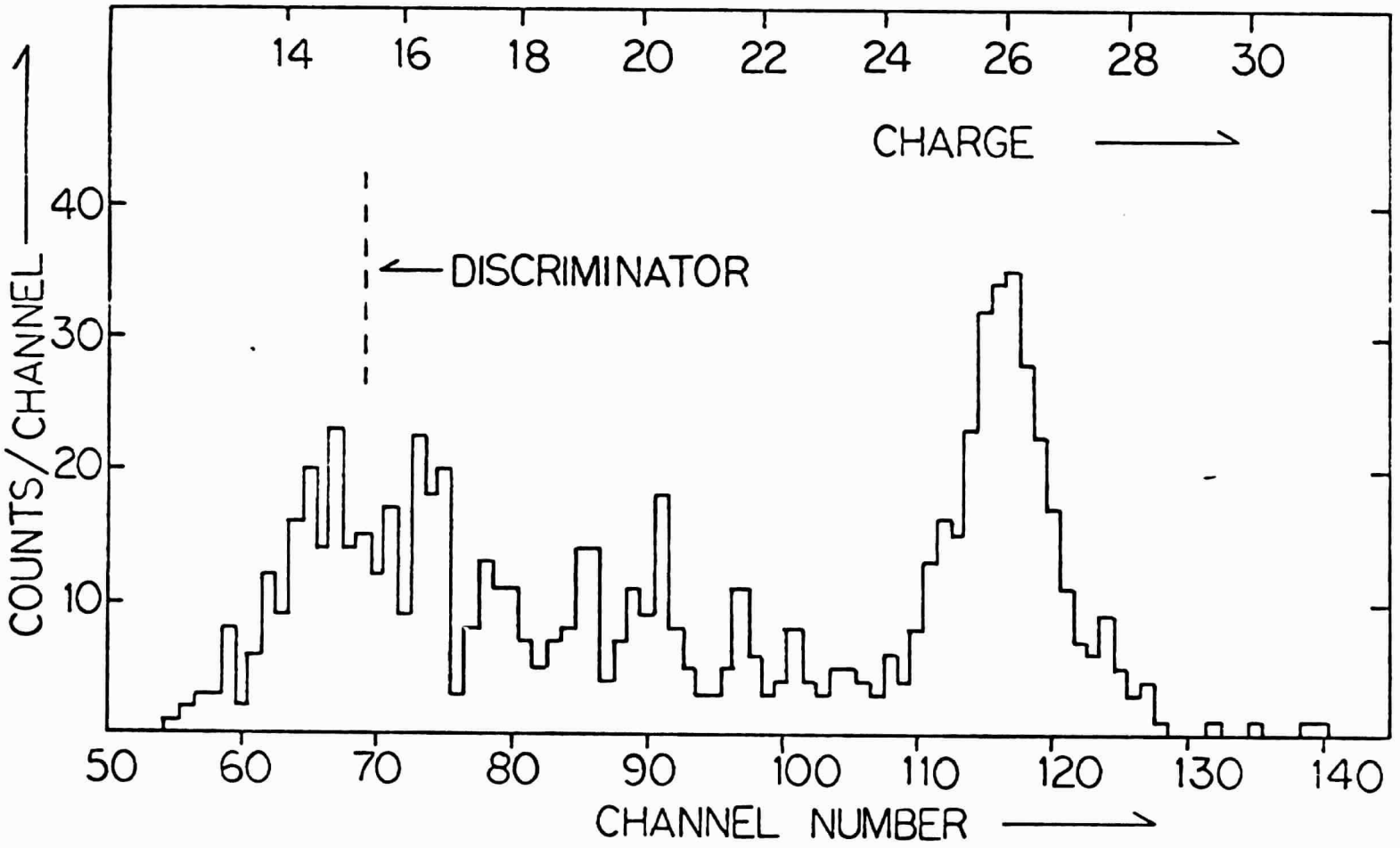
14
16
18
20
22
24
26
28
30
CHARGE
DISCRIMINATOR
COUNTS/CHANNEL
40
30
20
10
50
60
70
80
90
100
110
120
130
140
CHANNEL NUMBER

FIG - 6

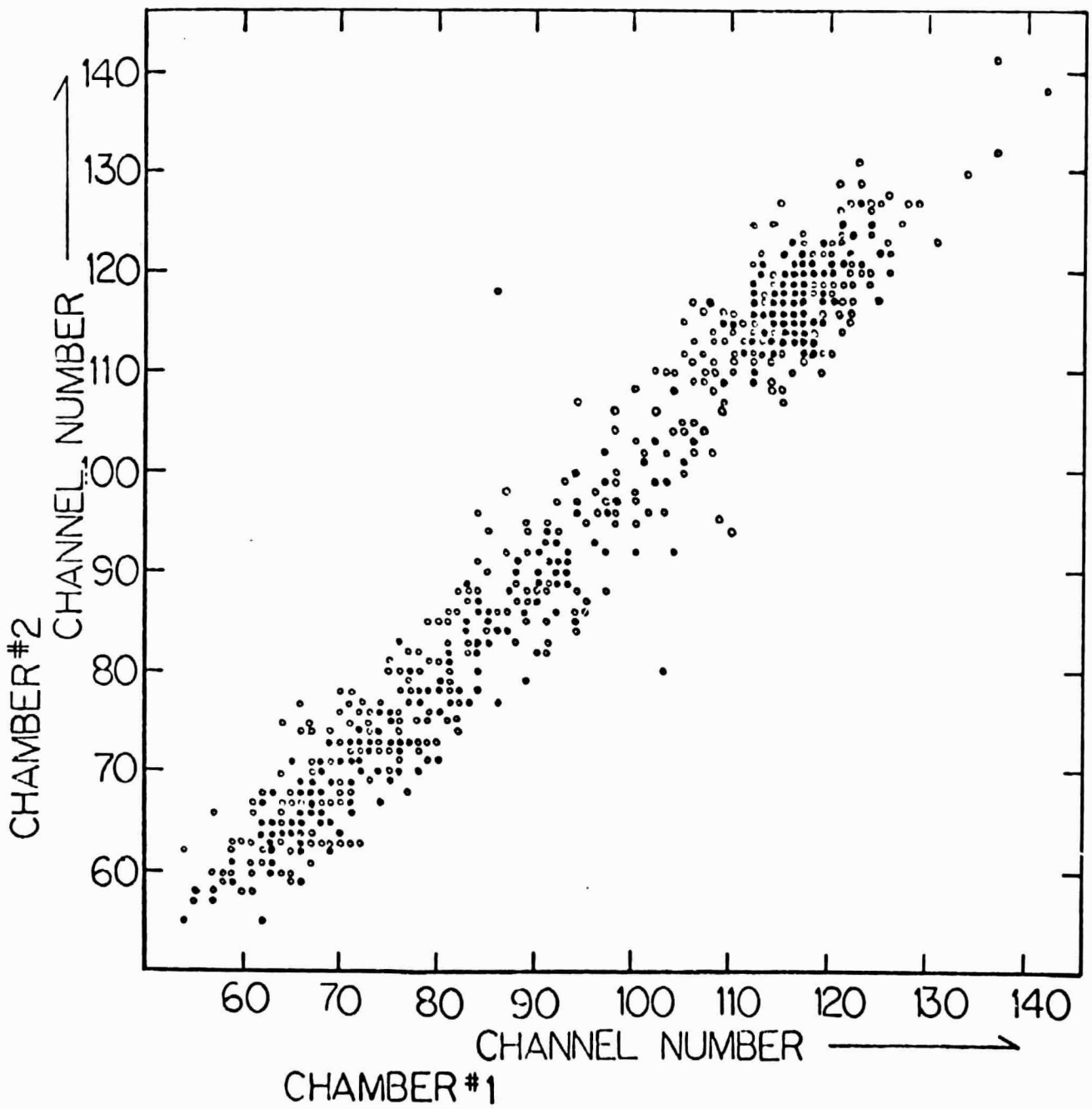
CHAMBER #2
CHANNEL NUMBER
140
130
120
110
100
90
80
70
60
60
70
80
90
100
110
120
130
140
CHANNEL NUMBER
CHAMBER #1

FIG - 7

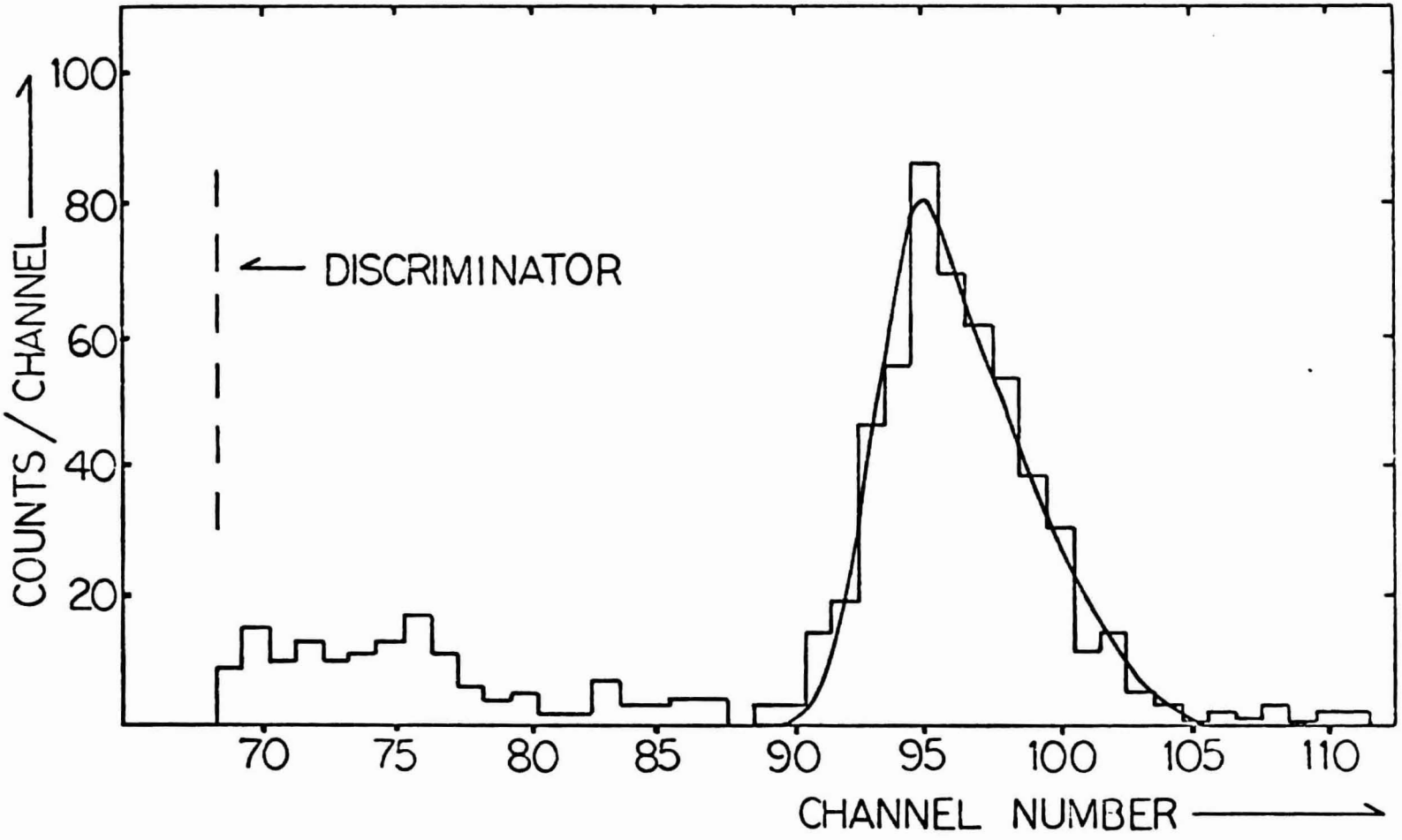
100
80
60
40
20
COUNTS / CHANNEL
DISCRIMINATOR
70
75
80
85
90
95
100
105
110
CHANNEL NUMBER